Biochimie 189 (2021) 1–12

Contents lists available at ScienceDirect

Biochimie

journal homepage: www.elsevier.com/locate/biochi

The allosteric protein interactions in the proton-motive function of mammalian redox enzymes of the respiratory chain

Giuseppe Capitanio [a], Francesco Papa [a], Sergio Papa [a, b, *]

[a] Department of Basic Medical Sciences, Neurosciences and Sense Organs, University of Bari "Aldo Moro", 70124, Bari, Italy
[b] Department of Biology and Evolution of Marine Organisms, Stazione Zoologica Anton Dohrn, 80121, Napoli, Italy

ARTICLE INFO

Article history:
Received 8 April 2021
Received in revised form
17 May 2021
Accepted 31 May 2021

Keywords:
Proton-motive activity
Respiratory chain
Allosteric protein interactions
Proton energy conversion
Mitochondria
Redox enzyme complexes

ABSTRACT

Insight into mammalian respiratory complexes defines the role of allosteric protein interactions in their proton-motive activity.

In cytochrome *c* oxidase (CxIV) conformational change of subunit I, caused by O_2 binding to heme a_3^{2+}-Cu_B^+ and reduction, and stereochemical transitions coupled to oxidation/reduction of heme *a* and Cu_A, combined with electrostatic effects, determine the proton pumping activity.

In ubiquinone-cytochrome *c* oxidoreductase (CxIII) conformational movement of Fe–S protein between cytochromes *b* and c_1 is the key element of the proton-motive activity.

In NADH-ubiquinone oxidoreductase (CxI) ubiquinone binding and reduction result in conformational changes of subunits in the quinone reaction structure which initiate proton pumping.

Contents

* Corresponding author. Department of Basic Medical Sciences, Neurosciences and Sense Organs, University of Bari "Aldo Moro", Policlinico, P.zza G. Cesare 11, 70124, Bari, Italy.
E-mail addresses: giuseppe.capitanio@uniba.it (G. Capitanio), francescopapa163@gmail.com (F. Papa), sergio.papa@uniba.it (S. Papa).

https://doi.org/10.1016/j.biochi.2021.05.018
0300-9084/

1. Introduction

From prokaryotes to humans the aerobic oxidation of NADH, produced in terminal metabolism, is catalysed in the canonical respiratory chain by the functional sequence of NADH-ubiquinone oxidoreductase (CxI), ubiquinone-cytochrome *c* oxidoreductase (CxIII) and cytochrome *c* oxidase (CxIV) enzyme complexes. The redox-driven proton-motive activity of each of the three complexes inserted in the coupling membrane results in proton uptake from a negative (N) space and proton release in a positive (P) space separated by the membrane thus generating the proton-motive force (pmf) which drives ATP synthesis in oxidative phosphorylation [1,2].

The molecular mechanisms of the proton-motive activity is a years lasting issue subject of extensive theoretical, experimental and molecular dynamics studies, continued by different groups nowadays, as quoted in the following sections.

A new insight into the coupling mechanism of mammalian redox enzymes has come in particular from methodological implementation of molecular structure analyses: application of serial femtosecond X-ray crystallography of complex IV and cryo-electron microscopy of complex I. The advances resulting from these and related studies of complex III define at molecular level the key role in the proton-motive activity of allosteric interactions in the core subunits of complex IV, complex III and complex I, inserted in the cristae of the mitochondrial inner membrane.

Allosteric interaction of distinct sites in proteins is a fundamental, widespread property by which proteins implement their functional activity [3].

2. Cytochrome *c* oxidase (CxIV)

Mammalian A1-type CxIV is composed of subunits I, II and III, forming the minimal functional core and 10 supernumerary subunits [4]. Cytochrome *c* binds to subunit II at the P membrane surface and delivers electrons to Cu_A in subunit II, heme *a* transfers electrons from Cu_A to the heme a_3-Cu_B BNC centre in subunit I. At BNC O_2 is reduced to two H_2O with consumption of four protons from the mitochondrial matrix (N) space. In addition up to four protons are pumped from the matrix into the intracristae (P) space (ICS) in the reduction by cyt.c^{2+} of O_2 to $2H_2O$ [4,5] (Fig. 1).

X-ray crystallography of bovine-heart [6] and prokaryotic CxIV [7] revealed the molecular structures of two conserved proton translocating pathways in subunit I. Pathway K which conducts from the N space to the BNC two protons consumed in the $O_H \rightarrow E$ and $E \rightarrow R$ steps of the catalytic cycle of oxygen reduction and the D pathway which conducts the other two protons in the $P_R \rightarrow F$ and $F \rightarrow O_H$ steps, details below and in Ref. [4]. In prokaryotic CxIV the D pathway appears to conduct also the pumped protons [8,9]. X-ray crystallography has identified in bovine CxIV a third (H) proton conduction pathway [6]. This formed by polar residues of subunit I helices XI and XII, constitutes a water channel from the N surface to the heme *a* domain. From there the H pathway continues with an hydrogen-bond network in subunits I and II reaching the P surface (Fig. 1) [4]. This H pathway, for which no equivalent structure is detectable in prokaryotic CxIV, has been proposed by the Yoshikawa's group to conduct pumped protons from the N to the P space [10,11], see also [12].

2.1. Spectral-electrochemical evidence of allosteric H^+/e^- coupling at heme a and Cu_A

Spectrophotometric and potentiometric analyses of purified, bovine-heart CxIV, carbon-monoxide ligated in which heme a_3 and

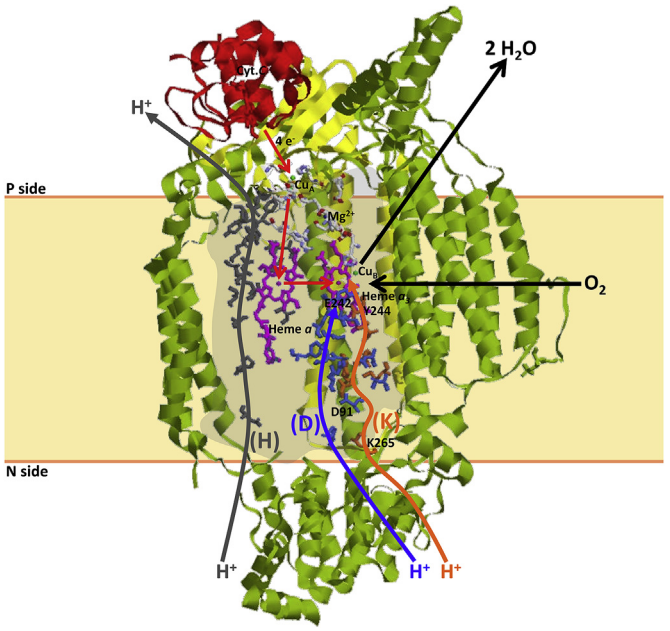

Fig. 1. X-ray crystallographic view perpendicular to the membrane plane of bovine-heart CxIV. The picture elaborated with RasTop 2.2 program and the PDB ID: 5IY5. Cytochrome *c* and CxIV subunit II are coloured in red and yellow, other CxIV subunits in green except subunit I, shaded grey. The porphyrin structures of hemes *a* and a_3, pink sticks, heme *c* as red sticks. Iron, copper and magnesium ions are pink, green and blue balls, respectively. The residues of K, D and H channels in subunit I are in orange, blue and dark grey sticks, the corresponding proton-conducting pathways are indicated by thick arrows. The K pathway starts at the N membrane side with conserved lysine (K265) and ends with conserved tyrosine (Y244) close to the BNC, the D pathway starts with conserved aspartate (D91) at the N membrane side and ends with conserved glutamate (E242) close to BNC. Electron transfer pathway indicated by red arrows. Oxygen entry and water exit are shown as black arrows. Subunits VIIa and VIIc and part of subunit III are not shown in the figure.

Cu_B are clamped in the reduced state, showed that oxidation-reduction of heme *a* and Cu_A are coupled with pK shifts of two acid/base groups at least [13]. This allosteric interaction results in the same pH dependence of the midpoint redox potentials of heme *a* and Cu_A, both more negative upon pH increase in the physiological range [13], with release of $\approx 1H^+$/mole CxIV upon full oxidation of both heme *a* and Cu_A [14]. In liposome-reconstituted purified bovine CxIV, CO-ligated as well as in the unligated state, H^+ translocation coupled to oxidation-reduction of heme *a* and Cu_A exhibited membrane vectoriality, i.e. release of $\approx 1H^+$ in the outer P space upon oxidation of both heme *a* and Cu_A and H^+ uptake from the intraliposomal N space upon their re-reduction [15].

Resonance Raman spectroscopy of CxIV [16] provided evidence of an hydrogen bond between the heme *a* porphyrin formyl and an amino acid residue in the apoprotein, later identified by X-ray crystallography as the conserved R38 (bovine numbering) of subunit I [6].

2.2. Redox-linked allosteric structural interactions revealed by X-ray crystallography

X-ray crystallography of purified bovine-heart CxIV [10,17,18] shows that in the fully oxidized crystals (Fig. 2A) the helical segment V380-L381-S382-M383 of subunit I is unwound with respect to the fully reduced crystals (Fig. 2B) with S382 OH getting close to the heme *a* farnesyl OH. The S382 movement is accompanied in the oxidized crystals by a 120° rotation of the farnesyl OH towards the S382 OH forming with it an hydrogen bond. The G49-

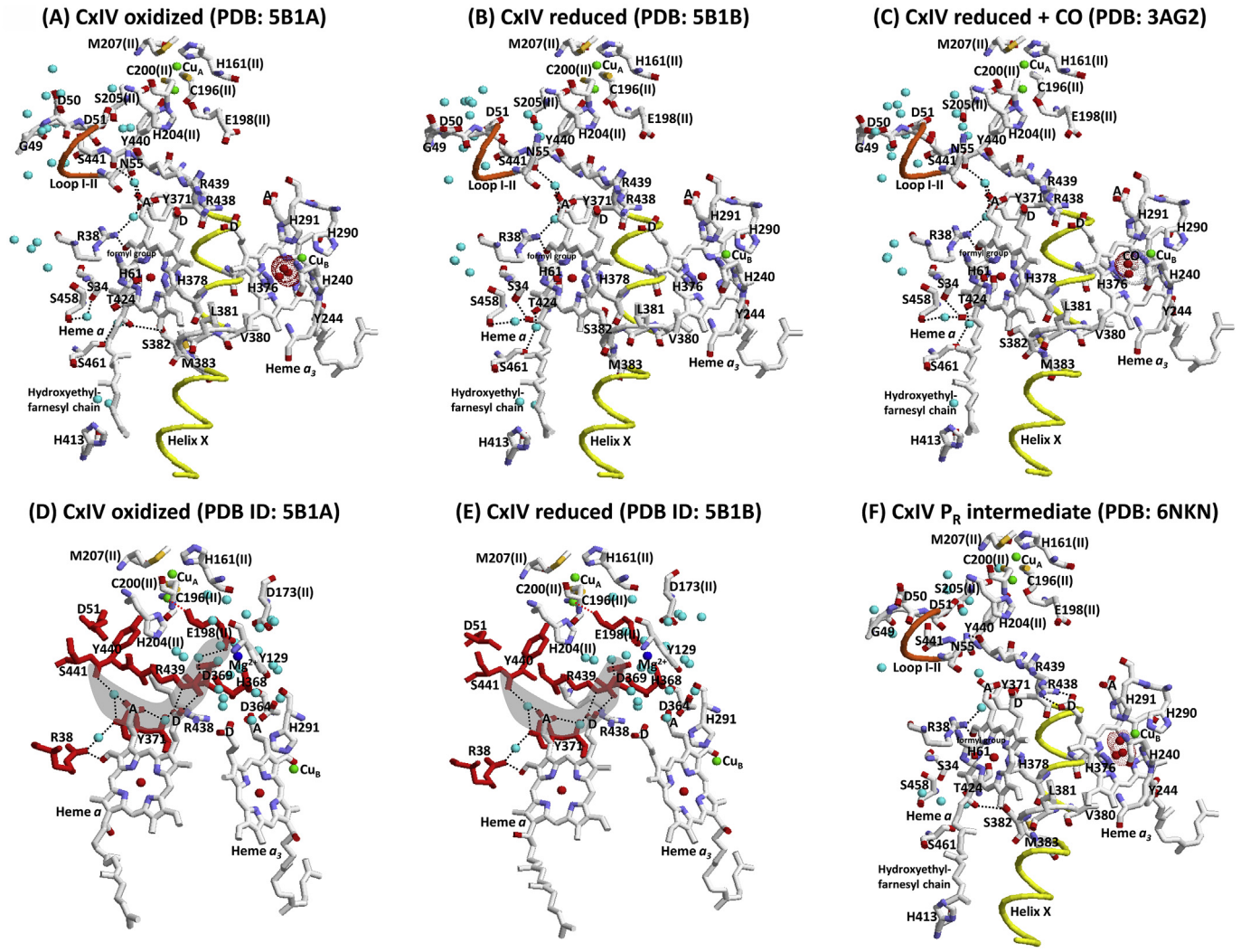

Fig. 2. X-ray crystal structures of bovine-heart CxIV in different redox and CO-ligated states. The crystals are from purified CxIV solubilized as homodimers in cholate [10,12,18]. Picture produced by RasTop 2.2 program and the PDB ID 5B1A, 5B1B and 3AG2 for fully oxidized (A), fully reduced (B) and fully reduced CO-ligated CxIV (C) [19] respectively. The same X-ray crystal structures of Fig. 2A and B were detected in the purified CxIV solubilized in 3-oxatridecyl-α-D-mannoside as active monomers [17] this showing that dimerization does not affect the structures, PDB ID: 6YJ3 and 6YJ4 for fully oxidized and fully reduced CxIV respectively. (D) Fully oxidized and (E) fully reduced X-ray crystal structures of the CxIV region above hemes *a* and a_3 [18]. Letters A and D are the hemes propionates. Helix X and loop I-II of subunit I are shown as trace mode in yellow and orange respectively. Hemes and residues are shown as sticks, iron and copper as red and green balls. The oxygen reduced-species and CO are shown as two red balls and a red and white balls respectively with van der Waals atomic radii. Small blue balls are H_2O molecules. Dotted lines indicate hydrogen bonds. In the oxidized (D) and reduced (E) structures above the hemes the E198-II residue ligand to Mg^{2+} is coordinated to Cu_A by the peptide carbonyl (red-dotted lines). The residues in red involved together with H_2O in a hydrogen bond network connecting E198-II/Mg^{2+}/H_2O cluster with R439-I to the propionate(s) of heme *a* porphyrin are shown in a grey area. In the reduced state the coordination angle of E198-II carboxyl to Mg^{2+} increases with respect to the oxidized state breaking a hydrogen bond between E198-II and a H_2O bonded to R439-I, resulting in a lower capacity of proton transfer between E198-II and R439-I (details in the text and [18]). In the P_R intermediate (F) the H pathway at the P side of heme *a*, helix X and loop I-II of subunit I are the same as those in (A).

D51 segment of subunit I loop I-II, exposed at the P surface in the reduced crystals (Fig. 2B) is in the oxidized crystals buried in the protein (Fig. 2A).The X-ray crystals of the fully reduced, carbon-monoxide ligated CxIV [19] (Fig. 2C) show that CO binding at the BNC results in the same unwinding of the subunit I helix segment V380-L381-S382-M383 detected in the fully oxidized crystals. Upon photodissociation of CO from Fea_3^{2+} in the reduced crystals, the plane of heme a_3 was shown by serial femtosecond X-ray crystallography to undergo a small rotation, its vinyl substituent pushed L381 of helix X and S382 was displaced from the vicinity of heme *a* farnesyl [11,20]. These findings show that the unwinding of helix X in the fully oxidized state is, in fact, due to O_2 binding at the BNC. In the fully reduced CO-ligated crystals the position of the heme *a* farnesyl and the conformation of the G49-D51 loop remained the same as in the fully reduced crystals (compare Fig.s 2B and 2C), showing that these conformational changes detected in the fully oxidized crystals (Fig. 2A) are due to oxidation of the redox centres. Fourier-transformed infrared spectroscopy provided evidence that these conformational changes are associated with oxidation of heme *a* or Cu_A [21]. It can be noted that the polar residues present in the bovine CxIV hydrogen-bond network at the P side of heme *a* are absent in prokaryotic CxIV [7,22]. The X-ray crystallography of *Rhodobacter sphaeroides* CxIV shows the unwinding in the fully oxidized crystals of the subunit I helix X, but there is no rotation of the heme *a* farnesyl OH which in both the reduced and oxidized crystals is oriented at the opposite side of the serine OH [22] (see Fig. 5 of [23]).

The X-ray crystals of fully oxidized and fully reduced bovine CxIV identify also at the P side of the BNC and heme *a* a Mg^{2+}-proton storage site [18] (Fig.s 2D and 2E). This site can accept

pumped protons translocated there from the N space. Mg^{2+} at this site is coordinated with the carboxylic group of subunit II E198 whose main chain carbonyl is coordinated with one copper of the binuclear Cu_A centre. Mg^{2+} is also hexacoordinated with two subunit I residues and water molecules [18]. This site is connected by an hydrogen-bond network to the heme *a* propionate(s) (see Fig. 2D) showing a structural basis for the H^+/e^- coupling shared by heme *a* and Cu_A revealed by the pH dependence of their redox potentials [13,14].

2.3. The proton-motive catalytic cycle

Binding of O_2 to BNC in the fully reduced CxIV generates an intermediate in which O_2, in a position between Fea_3 and Cu_B [10], can be transiently reduced to the superoxide [24] or to the peroxy species [25]. The O—O bond is then split by the delivery of one electron in the oxidation of Fea^{2+} and electron redistribution at the BNC with formation of the P_R species [25]. Delivery of a first electron from cyt.c^{2+} and uptake of one proton from the N space converts the P_R to the F intermediate of the catalytic cycle. On sequential delivery of three additional electrons from cyt.c^{2+} and consumption of three more protons from the N space, one each in the F → O_H, O_H → E and E → R with production of two H_2O the R state is reformed [4].

By time resolved optical absorption spectra and serial femtosecond X-ray crystallography an intermediate has been identified by Rousseau and coworkers [12] which is formed in bovine CxIV after mixing the fully reduced oxidase with an O_2 saturated buffer (Fig. 2F). This intermediate shows optical spectra of P_R and F compounds. The femtosecond crystal structures showed a number of conformational changes in the intermediate with respect to the R state (Compare Fig. 2F with Fig. 2B). The OH of the heme *a* farnesyl was rotated by 120° approaching at an hydrogen bond distance the OH of S382, which concomitantly moved towards the heme *a* farnesyl by unwinding of the V380-L381-S382-M383 helical segment of subunit I with formation of an hydrogen bond between the two. The rotation of the OH of heme *a* farnesyl reflected oxidation of Fea^{2+}, whilst Cu_A remained reduced [12]. The spectral and structural features of this compound thus identify it as an intermediate in the catalytic cycle involving oxidation of Fea^{2+}. Oxidation of Fea^{2+} to Fea^{3+} causes by electrostatic repulsion release in the P space of one proton from the heme *a* environment. Heme *a* oxidation determines also with the rotation of the hydroxyfarnesyl translocation, by the H pathway water channel, of one pumped proton from the N space to the Mg^{2+}-loading site [12]. Upon re-reduction of Fea^{3+} by cytochrome *c*, via Cu_A (P_R → F step) the proton that has been released from the heme *a* environment in the P space is replaced by translocation, via the hydrogen bond connecting the Cu_A and heme *a* environments of one proton from the Mg^{2+}-loading site. These translocation steps result thus in the effective pumping of one proton from the N to the P space. Three more protons, one each in F → O_H, O_H → E and E → R steps of the catalytic cycle will be pumped from the N to the P space upon transfer of each electron from cytochrome c^{2+} to O_2 bound at the BNC.

It is alternatively proposed by Yoshikawa et al. [11,21] that in the R state of the catalytic cycle the H pathway is open and four protons from the N space move in a water cavity to the Mg^{2+}-storage site. The water cavity is then closed upon O_2 binding at the BNC. In each of the four steps of the catalytic cycle the water cavity in the H pathway remains closed and four protons are released from the Mg^{2+}-storage site in the P space upon delivery of each electron from cytochrome c^{2+} to O_2. In either case in the overall catalytic cycle four protons are pumped by the H pathway and four protons conducted by the K and D pathways from the N space to the BNC are consumed in the reduction of O_2 to two H_2O.

A recent study [26] has shown that in *Saccharomyces cerevisiae* CxIV the point mutation N99D in the subunit I D pathway decoupled the proton pump. This indicates that in yeast CxIV the D pathway is involved in translocation of pumped protons. Mutations in yeast of amino acids in the N-side part of the putative H channel did not uncouple proton pumping [26]. It had on the other hand been shown that the point mutations D51N and S441P in subunit I H pathway in a human/bovine hybrid CxIV decoupled proton pumping [4]. It can be noted that the corresponding positions of Y440—I, S441—I and S205-II, which in mammalian CxIV are involved in the hydrogen-bond network of the H pathway at the P side of the heme *a* environment, are occupied in yeast by residues I440—I, P441—I and A230-II respectively. In the evolution course genetic introduction of polar residues in subunits I and II of high eukaryote CxIV has resulted in the formation of the proton conducting H pathway.

2.4. ATP induced allosteric inhibition of CxIV. Involvement of subunit IV-1

ATP depresses cytochrome *c* oxidation by the mitochondrial CxIV, as compared to the activity of ADP supplemented samples [27]. An ATP regulatory site has been detected at the N-side of mitochondrial CxIV [27]. A monoclonal antibody against the supernumerary subunit IV-1 prevented in solubilized mitochondria ATP inhibition of cytochrome *c* oxidation [27]. In purified bovine-heart CxIV removal by trypsin digestion of the subunit IV-1 N-terminal residues up to the sequence V5—V6—K7 (Fig. 3A) inhibited the rate of cytochrome *c* oxidation and decreased the H^+/e^- ratio of proton pumping in the liposome reconstituted CxIV [28].

MD analysis of murine CxIV indicated that ATP can bind through interaction of the β and γ phosphates with the hydroxyl moieties of S56 and S58 (murine numbering) of the N terminal region of subunit IV-1 [29] (Fig. 3A). Mutation of S58 to alanine abolished the inhibitory effect of ATP [29]. Phosphorylation of S58 by the mitochondrial matrix protein kinase A [30], promoted by cAMP produced in the matrix by soluble adenylate cyclase [31], prevented CxIV inhibition by ATP.

In the X-ray crystal structures of bovine-heart CxIV the N-terminal loop of subunit IV-1 appears close to the N-surface of subunit I (Fig. 3B). The V5—V6—K7 sequence is surrounded by water located at the entry mouths of subunit I proton channels. This sequence might facilitate entrance into the channels of matrix bulk phase protons. ATP binding at the subunit IV-1 Ser-site could, by allosteric interaction, depress the proton facilitating function of subunit IV-1 N-terminal sequence. The N-terminal loop of subunit IV-1 continues with an α-helix in the transmembrane region, ending with the C-terminal loop which protrudes in the P space in contact with the loop of subunit II where cytochrome *c* binds (Fig. 3B). An allosteric perturbation induced by ATP binding at the N-terminal loop and transmitted throughout all the subunit to the C-terminal loop could depress cytochrome *c* binding to subunit II inhibiting cytochrome *c* oxidation.

3. Ubiquinone-cytochrome *c* oxidoreductase (CxIII)

Cytochrome *b* ($b_{L(566)}$-$b_{H(562)}$), Rieske iron-sulphur protein, ISP [2Fe2S] and cytochrome c_1, conserved from prokaryotes to humans, constitute the minimal functional core of CxIII in which the redox proton-motive process takes place [32,33]. In the mammalian complex, which is always present as homodimer in the native and isolated state, there are eight supernumerary subunits [32]. The mechanism of the proton-motive activity in mammalian as well as prokaryotic CxIII is explained by the double version [32—34] of the

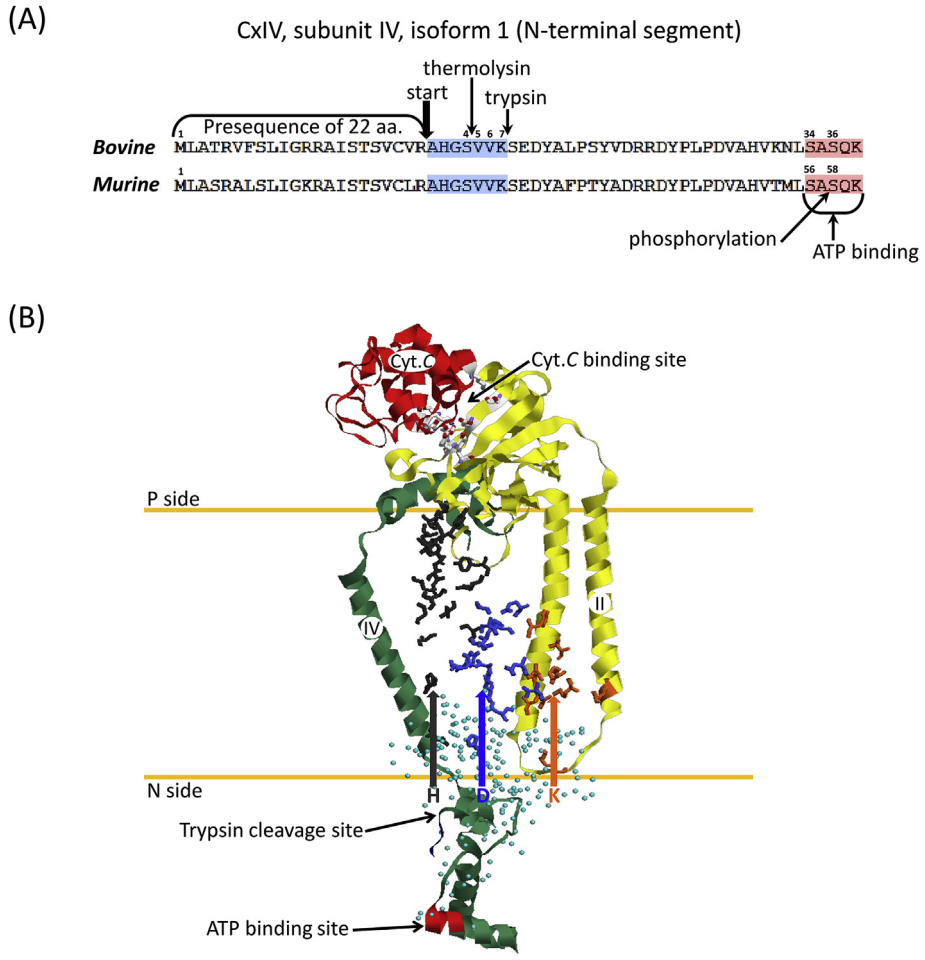

Fig. 3. N-terminal sequences of bovine and murine CxIV subunit IV-1 and X-ray crystallographic view of subunit IV-1 and II in bovine CxIV. (A) Residue numbered in bovine subunit IV-1 from Ala-1 of mature protein, from Met-1 of presequence in murine. The first residues of mature bovine IV-1 subunit in blue (AHGSVVK) were found to be removed by trypsin digestion, the first four (AHGS) by thermolysin [28]. The bovine segment, shown in red (SASQK), is the ATP binding site, S58 is phosphorylated by PKA as shown for the murine subunit [29]. (B) Crystallographic view perpendicular to the membrane plane of subunits IV-1 and II (RasTop 2.2 program, PDB ID: 5IY5) and cytochrome *c* coloured in green, yellow and red. In membrane spanning subunit I residues of K proton pathway in orange, D pathway in blue and H pathway in dark grey. The cytochrome *c* residues involved in binding to subunit II residues are shown as coloured sticks. The residues forming the ATP binding site in subunit IV-1 N loop are in red. The residues in subunit IV-1 removed by trypsin digestion are in blue. The entry mouth of the K, D and H proton channels are orange, blue and dark grey.

quinone (Q) cycle conceived by Mitchell [35]. In this, two quinols of the membrane pool [36] are sequentially oxidized by a split ISP [2Fe2S] process in which two electrons are transferred via cytochrome c_1 to cytochrome *c*, four protons are released in the intracristae (P) space and two electrons are cycled back by cytochrome *b* to reduce one quinone of the pool with the uptake of two protons from the matrix (N) space.

3.1. Features of CxIII disclosed by limited proteolysis

Papain digestion of the purified bovine-heart CxIII in the fully oxidized state was found to cleave off the N-terminal end of the supernumerary subunit 14-kDa [37,38], which is exposed at the N surface of the complex [39]. The complex so digested showed when reconstituted in phospholipid vesicles partial decoupling of proton pumping [37]. Papain digestion of the oxidized complex resulted also in small inhibition of electron flow and cleavage of the ISP with removal of sixty-three residues of the N-terminal moiety with detachment from the complex of the C-terminal moiety holding the [2Fe2S] centre. Reduction by ascorbate of the high E_m redox potential centres, [2Fe2S] and cytochrome c_1, increased the digestion of the ISP as well as of the 14-kDa subunit with more marked inhibition of electron flow. Papain digestion of CxIII [37] decreased also the g = 2.00, +100 mV EPR signal of a protein bound antimycin sensitive semiquinone detected in the complex [40].

3.2. X-ray crystallographic structures

X-ray crystals of purified bovine-heart [41,42] and chicken-heart [43] of homodimeric CxIII show that the ISP is interwound with the N-terminal moiety anchored in one monomer and the C-terminal moiety with the 2Fe2S centre (ISP-ED) protruding at the P surface of the other monomer (Fig. 4). The X-ray crystal structures show that inhibitors such as stigmatellin and UHDBT block the ISP-ED at the ubiquinol oxidation site relatively close to cytochrome *b* (b position) whilst inhibitors like myxothiazol and azoxystrobin block the ISP-ED in a position in which the 2Fe2S centre approaches the cytochrome c_1 heme at a distance which can allow kinetically competent electron transfer between the two (c_1 position) [43,44] (Fig. 4). It was also found in the *Rhodobacter capsulatus* CxIII that cleavage by thermolysin of the ISP segment linking the N and the C terminal moieties was prevented when the ISP-ED was blocked by stigmatellin in the b position [45]. These findings thus show that the redox state of the 2Fe2S centre determines the movement of

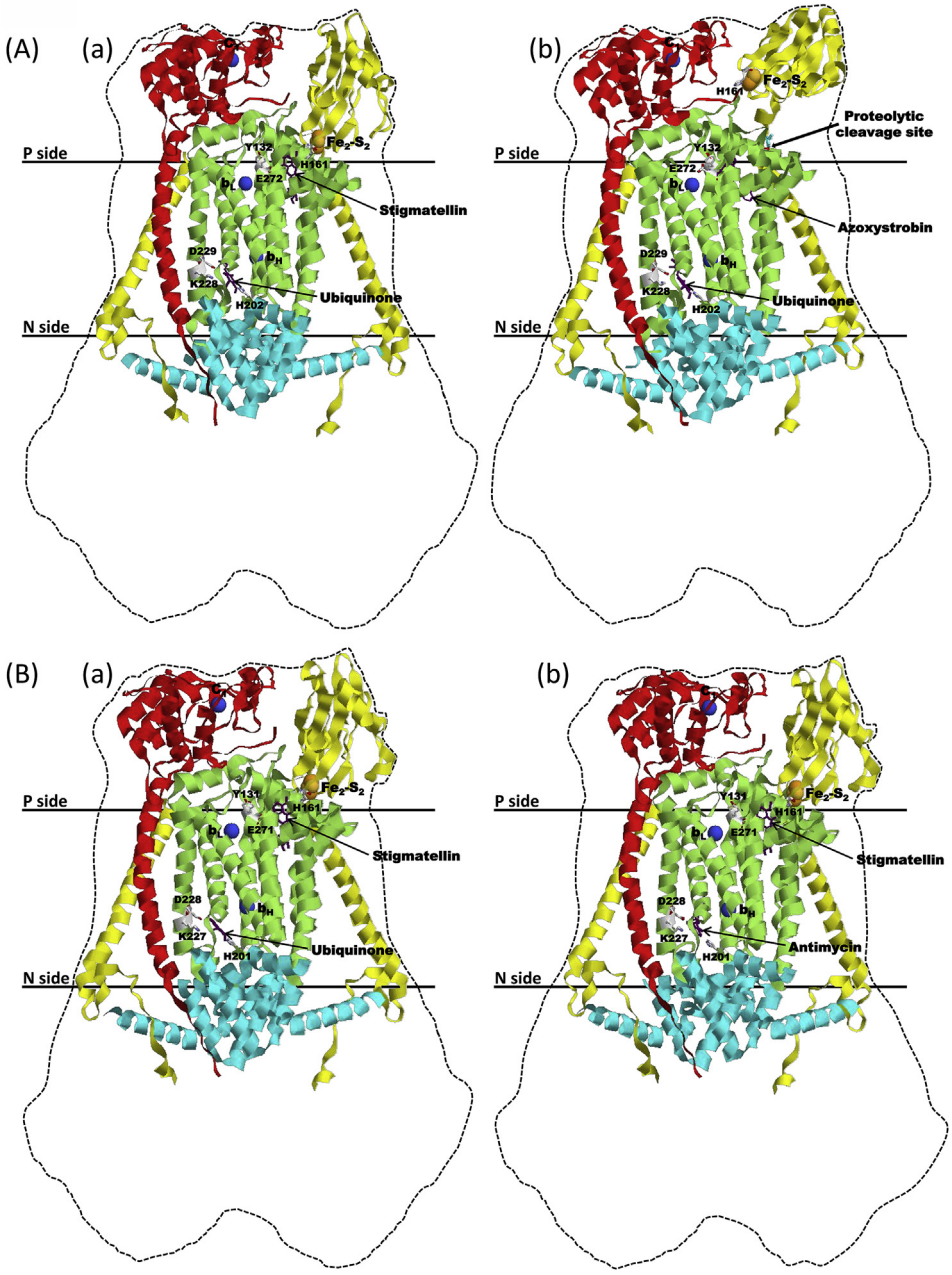

Fig. 4. X-ray structures of chicken (A) and bovine CxIII (B) ligated by inhibitors. Structures by RasTop 2.2, PDB ID: 3H1J, 3L71 for stigmatellin-ligated (A-a) and azoxystrobin-ligated (A-b) structures, PDB ID: 1PP9 and 1PPJ for stigmatellin (B-a) and stigmatellin plus antimycin-ligated (B-b) structures. In (A-a), (A-b) and (B-a) a quinone molecule (violet sticks) is bound at Q_i site from where it is displaced by antimycin (B-b). In structures (A-a), (B-a) and (B-b) a stigmatellin is bound at the Q_o site replaced by azoxystrobin in (A-b) (inhibitors violet sticks). Cytochrome *b* (green), cytochrome c_1 (red), Rieske ISP (yellow) and 14-kDa subunit (turquoise). Iron of b_L, b_H and c_1, blue balls; ISP Fe_2—S_2 centre, yellow-orange balls. CXIII is an homodimer, cytochrome *b* and cytochrome c_1 are shown only in one monomer. ISP moiety holding 2Fe2S (ED) is at the P surface of one monomer, its N-moiety is inserted in the other monomer. View in one monomer cytochrome *b*, c_1, ISP-ED of the other monomer and N-moiety of ISP (this shown in both monomers). Profile of CxIII dimers shown by dotted contour. Residues of Q_o and Q_i are coloured sticks. In (A-b) the papain cleavage site S63 (in red) and A64 (in turquoise).

the ISP-ED between the b and the c_1 positions. Stigmatellin or myxothiazol inhibit CxIII by blocking this movement as well as by competing with ubiquinol for the Q_o site (see also [46,47]).

3.3. The proton-motive catalytic cycle

(1) The benzenoid ring of a quinol of the membrane pool penetrates the oxidation site (Q_o) of CxIII at the P side with one hydroxyl group getting hydrogen bonded to a conserved ISP histidine, ligand of the [2Fe2S] cluster and the other hydroxyl group hydrogen bonded to conserved tyrosine and/or glutamic residues of cytochrome *b* [48]. At this site bound quinol is positioned between the [2Fe2S] cluster and heme b_L (b position). The configuration of this b position is shown in Fig. 4A-a, by the X-ray crystal structure of the Q_o site in the stigmatellin-ligated structure [43,44]. (2) Bound quinol donates its first electron to [2Fe2S] with transient formation of a spin-coupled [$2Fe^{2+}$2S]-SQ triplet state [49]. The reduced [2Fe2S] cluster moves since of the ISP-ED conformational change from the b position to that closer to the cytochrome c_1 heme (c_1 position). The configuration of this c_1 position is shown in

Fig. 4A-b, by the X-ray crystal structure of the Q_o site in the azoxystrobin-ligated [50] or myxothiazol-ligated [44] structures. The first proton from quinol oxidation is released in the P space and a second EPR signature of SQ left in the environment of b_L is detected [49]. (3) SQ donates the second electron to b_L^{3+}, quinone leaves the site and the second proton is transiently held by cytochrome *b* lysine and/or glutamic. (4) The second electron is transferred from b_L^{2+} to b_H^{3+} located in the central/N region of cytochrome *b* and the second proton is released in the P space. (5) The first electron is transferred from [$2Fe^{2+}2S$] to cytochrome c_1 and from this to cytochrome *c* bound at the P side of CxIII; reduced cytochrome *c* leaves the complex [51]. The [$2Fe^{3+}2S$] cluster moves back to the b position. (6) According to the Q cycle a quinone of the pool bound at the N side of CxIII [52,53] is reduced by b_H^{2+} to SQ. In the double Q cycle, oxidation of a second quinol of the pool, by the same steps followed by oxidation of the first, results in the reduction of SQ held at the Q_i site with the overall uptake of two protons from the N space and quinol release in the membrane pool.

The molecular mechanism of quinone binding at the Q_i site, its reduction to quinol and release of quinol in the membrane pool have been analyzed by X-ray crystal structures [52] and atomistic molecular dynamic simulations [53]. According to the mechanism(s) proposed lysine, aspartic and histidine residues of cytochrome *b* form hydrogen bonds to the two carbonyl oxygen of an incoming quinone through structured H_2O [52] or directly [53]. Hydrogen bonding raises the midpoint potential of bound quinone thus promoting its reduction by b_H^{2+}. The residues hydrogen-bonded to the quinone mediate also transfer of the two protons from the N space which are utilized in the reduction of quinone to quinol. Upon quinone reduction the above hydrogen-bond network breaks down and quinol is released in the membrane pool. The 14-kDa subunit, located at the N surface of CxIII [39,41] could be involved in binding of quinone of the membrane pool at the N surface thus promoting its productive access to the Q_i site.

The molecular specific structures of the distinct quinol oxidation and quinone reduction sites and the redox chemistry of the quinone bound at the two sites are also aspects which require further clarification.

4. NADH-ubiquinone oxidoreductase (CxI)

4.1. Protein structure and redox carriers

Mammalian CxI is formed of a minimal functional core of 14 subunits, conserved from prokaryotes [54] to humans and 31 supernumerarary subunits [55–57] (Fig. 5A). Oxidation of one molecule of NADH in the mitochondrial matrix (N) space by one molecule of ubiquinone of the membrane pool [36] is coupled with pumping of four protons from the N to the P space [58]. The cryo-EM of mammalian CxI [55–57] shows an overall L-shaped structure of CxI formed by a N-side peripheral sector (PA) protruding in the N space and a membrane integral sector (MD) with a variable tilting angle in open-closed transition [57]. The PA sector is formed of seven subunits with NADH binding at the tip and a chain of Fe–S centres which transfer by the last N2–FeS centre of subunit PSST the two electrons from NADH to the quinone, likely one at a time with intermediate semiquinone production [59].

EPR spectral analysis of energy-coupled bovine heart mitochondrial inner membrane vesicles [60] showed two anionic semiquinone signatures, a fast relaxing one, highly sensitive to rotenone and to uncouplers (SQ_{NF}, $g = 2.05$) and a slow relaxing one (SQ_{NS}), less sensitive to rotenone and uncoupler insensitive. Spin-spin interaction of SQ_{NF} with the N2–FeS centre allowed to estimate a distance of 8–11 Å between the two. Uncoupler sensitive SQ_{NF} was also detected in steady-state electron flow from NADH to quinone in purified bovine heart CxI reconstituted in tightly-coupled proteoliposomes [61]. It is not clear if the two EPR semiquinone signatures correspond to two different protein-bound states of one or to two quinones [62,63].

The quinone reaction structure at the interface of PA and MD sectors consists of PSST and 49-kDa subunits shared with the PA sector and ND3, ND1, ND6 and ND4L subunits shared with the MD sector, these last three subunits forming a putative trasmembrane proton channel (channel E) [57] (see also [54,64]). In the MD sector there are three transmembrane subunits, ND2, ND4 and ND5 [57], with a structure analogous to the Na^+/H^+ antiporters of the plasma membrane [65]. These three subunits are arranged in a parallel sequence each with two discontinuous half-transmembrane helices (TMH), a N-terminal one extending from the N surface and a C-terminal one extending to the P side, connected by conserved Lys/Glu residues located between the two in the middle of the membrane-spanning dimension [57] (Fig. 5A).

The cryo-EM of mammalian CxI [57,66] (see also [64]) shows a sequence of structured water and hydrophilic residues which extends from the quinone reaction structure through the middle of the entire MD to the Lys/Glu residues in each of the ND2, ND4 and ND5 subunits.

4.2. The molecular mechanism of the proton-motive activity

Cryo-EM analysis of ovine CxI has revealed marked conformational changes of several loops of subunits of the quinone chamber in the open-closed structure transition of the complex [57] (Fig. 5B). On the basis of these conformational changes Sazanov's group has proposed a detailed coupling mechanism of mammalian CxI [57].

The cryo-EM structures of the open state showed opening of loops in the 49-kDa and PSST subunits, which form the deep cavity of the quinone chamber close to the N2–FeS centre, and ND1 TMHs 5–6 in the shallow part of the quinone chamber.

The open structure will allow quinone entry, binding and reduction in the deep cavity by the N2–FeS centre. Reduction of quinone results in closure of the opened loops and movement of quinol from the deep to the shallow site(s) of the chamber and release in the membrane pool. Reduction of quinone is proposed to involve protonation of Q^{2-} by sequential H^+ transfer from D160 and H59 of the 49-kDa subunit, reprotonated in turn by E34 and E70 of the ND4L subunit (Fig. 5B, bottom). Their negative charge induces pumping of one proton by the E pathway and would propagate to the middle of the ND2, ND4 and ND5 subunits inducing pumping of additional three protons per mole of NADH oxidized [57]. This last aspect needs however further study [57,67].

Delivery of a first electron from the N2–FeS centre to quinone involves likely intermediate semiquinone production. This semiquinone may be the $\Delta\tilde{\mu}H^+$-sensitive anionic $SQ^{\bullet-}{}_{NF}$ detected by EPR spectroscopy in bovine heart CxI [60,61]. $SQ^{\bullet-}{}_{NF}$ will bind at the deep site of the quinone chamber near the N2–FeS centre, possibly stabilized by cooperative H^+/e^- coupling at the N2–FeS centre [62,68]; its negative charge can trigger the negative-charge wave inducing proton pumping. Delivery of the second electron by the N2–FeS centre reduces $SQ^{\bullet-}{}_{NF}$ to quinol with the uptake of two protons. Neutral quinol moves from the deep site to the shallow site and leaves the complex.

The nature of the $\Delta\tilde{\mu}H^+$-insensitive $SQ^{\bullet-}{}_{NS}$, detected by EPR spectroscopy in addition to the $\Delta\tilde{\mu}H^+$-sensitive $SQ^{\bullet-}{}_{NF}$ in bovine [60] and *E. coli* CxI [69] remains to be clarified.

5. The overall proton energy conversion flow in mammalian mitochondria

Mammalian CxI, CxIII and CxIV assembled as supercomplexes

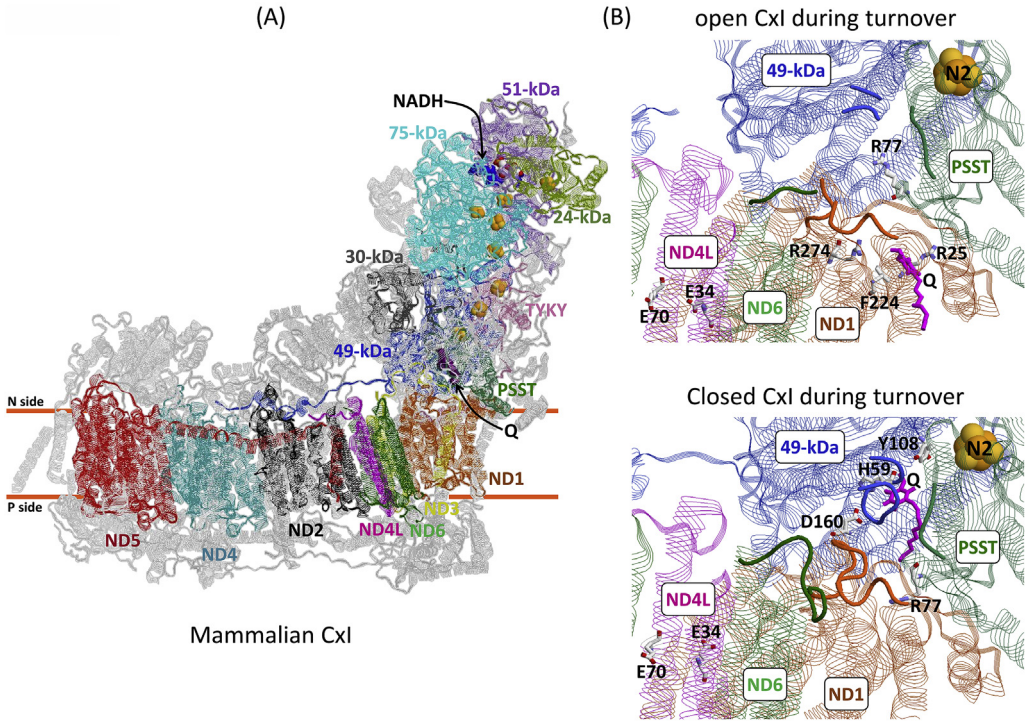

Fig. 5. (A) X-ray crystal structure of the ovine CxI. (B) View of the quinone chamber in open and closed states during turnover. Structures by RasTop 2.2 program, PDB ID: 6ZKC whole structure and closed state, 6ZKD open state. (A) Supernumerary subunits are in grey. FMN (red and white), NADH (blue), quinone (violet) and FeS clusters (yellow and orange). The structure is viewed perpendicular to the membrane plane. (B) 49-kDa, PSST, ND1, ND6 and ND4L subunits, quinone molecule in violet, N2–FeS centre yellow-orange balls. Some residues are presented as coloured sticks. Areas showing conformational changes in ND6, ND1, PSST and 49-kDa subunits in open-closed transition are shown in trace mode. In the open state quinone binding to the shallow site is shown with residues, in particular F224 belonging to ND1 subunit, close to quinone. In the closed state quinone binding to the deep site is shown with residues belonging to 49-kDa subunit.

[70–72] are clustered in cristae of the inner mitochondrial membrane (Fig. 6).

Dimers or oligomers of the F_oF_1 ATP synthase (CxV) [73,74] located at the apices of cristae contribute to their formation [75]. Cristae are joined to the boundary inner membrane (BIM) by junctions (CJ), which form a narrow cleft delimiting an intracristae space (ICS) with a high content of cytochrome *c* [76] (Fig. 6). Advanced super-resolution nanoscopy analyses show that mammalian individual cristae are dynamic structures with high capacity of proton energy conversion [77]. The functional unit of mitochondrial oxidative phosphorylation is composed of dimeric ATP synthase flanked by the adenine-nucleotide carrier, the phosphate carrier and CxI-CxIII$_2$-CxIV supercomplex (Fig. 6). In the phosphorylating state oxidation of two NADH molecules in two turnovers of CxI and CxIII and a catalytic cycle of CxIV reduces O_2 to two H_2O; a total of twenty protons are taken up by the three redox complexes from the matrix space and twenty protons are expelled at the intracristae side. Backwards translocation of eighteen protons, thirteen by the ATP synthase [78,79] and five by the phosphate carrier drives the synthesis of five ATP molecules at the matrix side [80], two protons leak back likely mediated by the uncoupler protein.

The supercomplexes favour shuttling of ubiquinone between CxI and CxIII [36] and cytochrome *c* between CxIII and CxIV. Under conditions of high ATP synthase activity protons pumped by the redox complexes can diffuse laterally to the synthase along the membrane surface [2,81,82] this limiting in the respiring steady-state establishment of bulk phase electrochemical proton gradient ($\Delta\tilde{\mu}H^+$), which is also contained by its dissipation by the uncoupler protein [83]. A high $\Delta\tilde{\mu}H^+$ increases the reduction level of quinone of the pool which can also depress the activity of CxII (succinate ubiquinone oxidoreductase). The proton pump of CxIV slips at high turnover rates of respiratory electron transfer [84,85], this contributing to contain establishment of a limiting bulk phase $\Delta\tilde{\mu}H^+$ at high reductive pressure imposed on the respiratory chain. When the matrix ATP/ADP concentration ratio increases markedly, upon saturation of ATP utilization in endergonic processes and net production of ATP is depressed, ATP binding at the matrix loop of CxIV subunit IV-1 results in allosteric depression of ferrocytochrome *c* oxidation and proton pumping efficiency in CxIV. Containment of a limiting bulk phase $\Delta\tilde{\mu}H^+$, not utilized in ATP synthesis prevents enhanced reduction level of CxI and CxIII redox intermediates, oxidizable by O_2 resulting in oxidative stress, and excessive production of saturated fatty acids and cholesterol supported by $\Delta\tilde{\mu}H^+$-driven transhydrogenation of NADH to $NADP^+$ [86]. Under conditions of elevated cellular Ca^{2+} concentration the electrical component of $\Delta\tilde{\mu}H^+$ raises mitochondrial Ca^{2+} uptake by the IM uniporter with opening of the IM permeability transition pore and possible mitochondrial dysfunctions [87–89]. In humans ATP production by oxidative phosphorylation is continually adapted to cover current changing requirements. Cyclic AMP produced in the mitochondrial matrix by the soluble adenylate cyclase [31], promotes phosphorylation by protein kinase (PKA) of CxIV subunit IV-1, preventing ATP inhibition of CxIV [29]. Phosphorylation by PKA of the Arg-Val-Ser sequence in the C-terminal moiety of CxI supernumerary subunit NDUSF4 is involved in CxI assembly and activity [90]. Genetic disorders destroying this phosphorylation site are associated with different neurological disorders [90]. In astrocytes cannabinoid activation of type-1 mitochondrial receptors inhibits phosphorylation of the NDUFS4 subunit decreasing the stability and activity of CxI [91].

An issue for future investigations is also the role of the numerous supernumerary subunits of mammalian CxI, CxIII and CxIV in their function and regulation in particular by signal

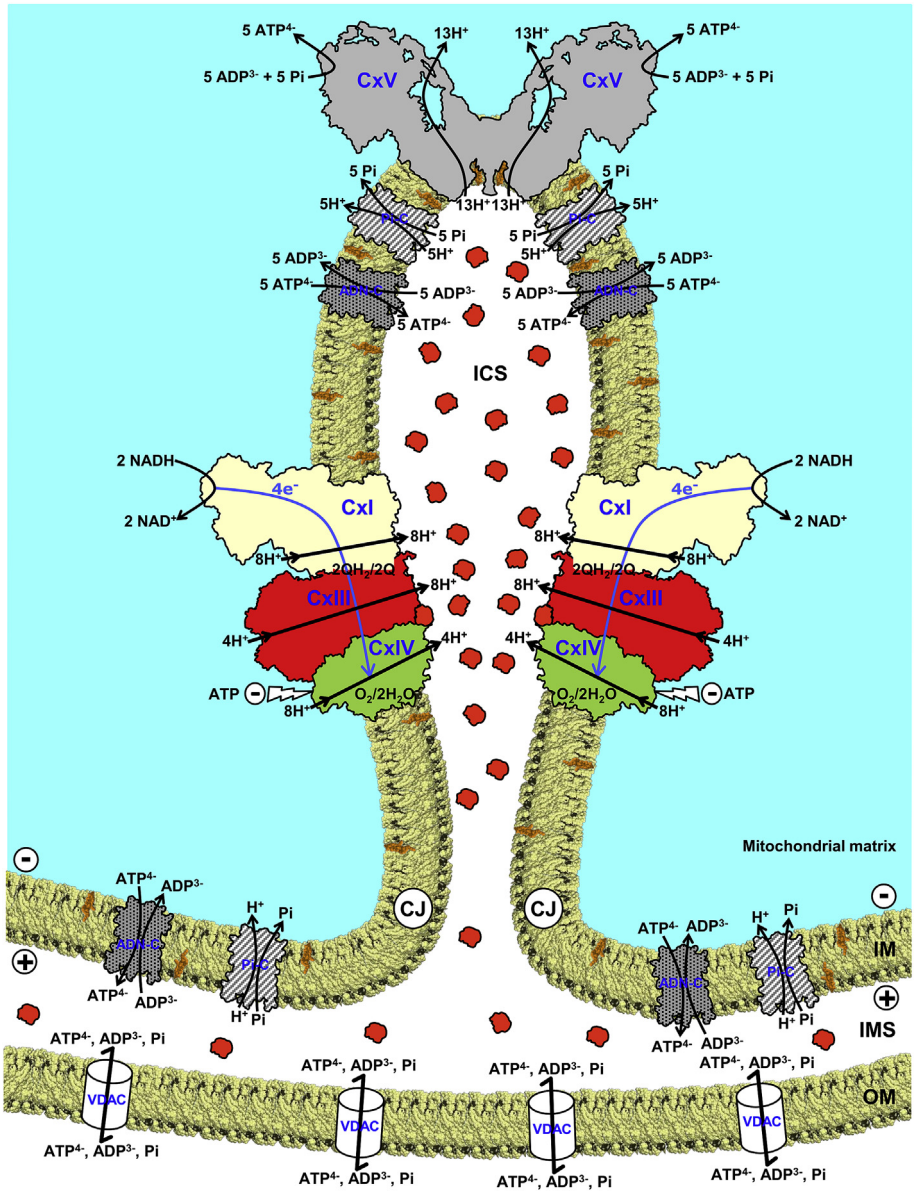

Fig. 6. The proton energy conversion flow in mammalian mitochondria. The profiles of CxI, $CxIII_2$, CxIV and cytochrome *c*, shown in their natural colours and the ATP synthase dimer are from the PDB ID: 5XTD, 5XTE, 5Z62, 1HRC and 6B8H, respectively. In addition to the conserved core subunits there are 10 supernumerary subunits in CxIV, 8 in CxIII and 31 in CxI. The intracristae space (ICS) has a high content of cytochrome *c* promoting electron transfer from CxIII to CxIV. Cristae are joined to the boundary inner membrane (BIM) by junctions delimiting a narrow cleft. The crystallographic profile of the ADN-carrier and that of the Pi-carrier (see also [92]), deduced from its structure, are shown in the inner mitochondrial membrane (IM). ADN-carrier transports ADP from the intermembrane space (IMS) and the intracristae space (ICS) to F_1 in exchange with ATP. The VDAC pore in the outer mitochondrial membrane (OM) allows diffusion of adenine nucleotides and substrates between the cytosol and the IMS.

transduction pathways.

6. Conclusions

(I) The advanced structural analyses of mammalian CxIV, CxIII and CxI of the respiratory chain define the allosteric conformational interactions in the core subunits of the enzymes providing the molecular structures of their proton-motive activity.

In cytochrome *c* oxidase (CxIV) conformational change of subunit I, caused by O_2 binding to heme a_3^{2+}-Cu_B^+ and reduction, and stereochemical transitions coupled to oxidation/reduction of heme *a* and Cu_A, combined with electrostatic effects, determine the proton pumping activity.

The key element of the proton-motive activity of CxIII is the redox coupled, reversible conformational movement of the ISP-[2Fe–2S] centre between cytochromes *b and* c_1 by which two quinols of the membrane pool are sequentially oxidized, two electrons are transferred to cytochrome *c*, four protons are released in the P space and two electrons are cycled back by cytochrome *b* to reduce one quinone of the pool with uptake of two protons from the N space.

Cryo-EM analysis of mammalian CxI has revealed conformational changes of subunits of the quinone reaction structure caused by quinone binding and reduction. It has been proposed that protonation of reduced quinone by proton transfer from residues of these subunits, preceding proton consumption from the N space,

generates a negative charge wave which induces proton pumping by membrane sector subunits.

(II) The overall proton-motive activity of CxI, CxIII and CxIV, associated in supercomplexes, is organized in the cristae of the mitochondrial inner membrane so to optimize the use of the proton-motive force (pmf) to drive ATP synthesis limiting in the respiring steady-state establishment of bulk phase electrochemical proton gradient ($\Delta\tilde{\mu}H^+$). This can otherwise enhance the reduction level of CxI and CxIII redox intermediates, oxidizable by O_2 with generation of free radicals, and raise mitochondrial Ca^{2+} uptake with opening of the inner membrane permeability transition pore and possible mitochondrial dysfunctions.

Authors contributions

Giuseppe Capitanio: analysis and interpretation of data, contribution to draft the article. Francesco Papa: critical scrutiny of literature. Sergio Papa: conception and design of the study, analysis and interpretation of data, drafting the article.

Funding

This work was supported by grants to S.P. from Ministero dell'Istruzione, dell'Università e della Ricerca MIUR, Italy. National Network for human proteomics, FIRB-Merit N_o. RBNE08HWLZ012 and grants from University of Bari to G.C. and F.P.

Declaration of competing interest

The authors declare no competing interests.

References

[1] P.D. Boyer, B. Chance, L. Ernster, P. Mitchell, E. Racker, E.C. Slater, Oxidative phosphorylation and photophosphorylation, Annu. Rev. Biochem. 46 (1977) 955–966, https://doi.org/10.1146/annurev.bi.46.070177.004515.

[2] S. Papa, G. Capitanio, F. Papa, The mechanism of coupling between oxido-reduction and proton translocation in respiratory chain enzymes, Biol. Rev. 93 (2018) 322–349, https://doi.org/10.1111/brv.12347.

[3] J. Monod, J.P. Changeux, F. Jacob, Allosteric proteins and cellular control systems, J. Mol. Biol. 6 (1963) 306–329, https://doi.org/10.1016/S0022-2836(63)80091-1.

[4] S. Yoshikawa, A. Shimada, Reaction mechanism of cytochrome *c* oxidase, Chem. Rev. 115 (2015) 1936–1989, https://doi.org/10.1021/cr500266a.

[5] M. Wikstrom, Proton pump coupled to cytochrome *c* oxidase in mitochondria, Nature 266 (1977) 271–273, https://doi.org/10.1038/266271a0.

[6] T. Tsukihara, H. Aoyama, E. Yamashita, T. Tomizaki, H. Yamaguchi, K. Shinzawa-Itoh, R. Nakashima, R. Yaono, S. Yoshikawa, The whole structure of the 13-subunit oxidized cytochrome c oxidase at 2.8 Å, Science 272 (1996) 1136–1144, https://doi.org/10.1126/science.272.5265.1136.

[7] S. Iwata, C. Ostermeier, B. Ludwig, H. Michel, Structure at 2.8 Å resolution of cytochrome *c* oxidase from *Paracoccus denitrificans*, Nature 376 (1995) 660–669, https://doi.org/10.1038/376660a0.

[8] A.A. Konstantinov, S. Siletsky, D. Mitchell, A. Kaulen, R.B. Gennis, The roles of the two proton input channels in cytochrome *c* oxidase from *Rhodobacter sphaeroides* probed by the effects of site-directed mutations on time-resolved electrogenic intraprotein proton transfer, Proc. Natl. Acad. Sci. U.S.A. 94 (1997) 9085–9090, https://doi.org/10.1073/pnas.94.17.9085.

[9] V. Sharma, G. Enkavi, I. Vattulainen, T. Rog, M. Wikstrom, Proton-coupled electron transfer and the role of water molecules in proton pumping by cytochrome *c* oxidase, Proc. Natl. Acad. Sci. U.S.A. 112 (2015) 2040–2045, https://doi.org/10.1073/pnas.1409543112.

[10] S. Yoshikawa, K. Shinzawa-Itoh, R. Nakashima, R. Yaono, E. Yamashita, N. Inoue, M. Yao, M.J. Fei, C.P. Libeu, T. Mizushima, et al., Redox-coupled crystal structural changes in bovine heart cytochrome c oxidase, Science 280 (1998) 1723–1729. https://doi:10.1126/science.280.5370.1723.

[11] A. Shimada, M. Kubo, S. Baba, K. Yamashita, K. Hirata, G. Ueno, T. Nomura, T. Kimura, K. Shinzawa-Itoh, J. Baba, et al., A nanosecond time-resolved XFEL analysis of structural changes associated with CO release from cytochrome c oxidase, Sci. Adv. 3 (2017), e1603042. https://doi:10.1126/sciadv.1603042.

[12] I. Ishigami, A. Lewis-Ballester, A. Echelmeier, G. Brehm, N.A. Zatsepin, T.D. Grant, J.D. Coe, S. Lisova, G. Nelson, S. Zhang, et al., Snapshot of an oxygen intermediate in the catalytic reaction of cytochrome *c* oxidase, Proc. Natl. Acad. Sci. U.S.A. 116 (2019) 3572–3577, https://doi.org/10.1073/pnas.1814526116.

[13] N. Capitanio, G. Capitanio, M. Minuto, E. De Nitto, L.L. Palese, P. nicholls, S. Papa, Coupling of electron transfer with proton transfer at heme *a* and Cu_A (redox Bohr effects) in cytochrome *c* oxidase. Studies with the carbon monoxide inhibited enzyme, Biochemistry 39 (2000) 6373–6379, https://doi.org/10.1021/bi0003137.

[14] N. Capitanio, G. Capitanio, D. Boffoli, S. Papa, The proton/electron coupling ratio at heme a and Cu_A in bovine heart cytochrome c oxidase, Biochemistry 39 (2000) 15454–15461, https://doi.org/10.1021/bi001940z.

[15] G. Capitanio, P.L. Martino, N. Capitanio, S. Papa, Redox Bohr effects and the role of heme *a* in the proton pump of bovine heart cytochrome *c* oxidase, Biochim. Biophys. Acta 1807 (2011) 1287–1294, https://doi.org/10.1016/j.bbabio.2011.02.004.

[16] G.T. Babcock, P.M. Callahan, Redox-linked hydrogen bond strength changes in cytochrome *a*: implications for a cytochrome oxidase proton pump, Biochemistry 22 (1983) 2314–2319, https://doi.org/10.1021/bi00279a002.

[17] K. Shinzawa-Itoh, T. Sugimura, T. Misaki, Y. Tadehara, S. Yamamoto, M. Hanada, N. Yano, T. Nakagawa, S. Uene, T. Yamada, et al., Monomeric structure of an active form of bovine cytochrome *c* oxidase, Proc. Natl. Acad. Sci. U.S.A. 116 (2019) 19945–19951, https://doi.org/10.1073/pnas.1907183116.

[18] N. Yano, K. Muramoto, A. Shimada, S. Takemura, J. Baba, H. Fujisawa, I. Mochizuk, K. Shinzawa-Itoh, E. Yamashita, T. Tsukihara, et al., The Mg^{2+}-containing water cluster of mammalian cytochrome *c* oxidase collects four pumping proton equivalents in each catalytic cycle, J. Biol. Chem. 291 (2016) 23882–23894, https://doi.org/10.1074/jbc.M115.711770.

[19] K. Muramoto, K. Ohta, K. Shinzawa-Itoh, K. Kanda, M. Taniguchi, H. Nabekura, E. Yamashita, T. Tsukihara, S. Yoshikawa, Bovine cytochrome *c* oxidase structures enable O_2 reduction with minimization of reactive oxygens and provide a proton-pumping gate, Proc. Natl. Acad. Sci. U.S.A. 107 (2010) 7740–7745, https://doi.org/10.1073/pnas.0910410107.

[20] I. Ishigami, N.A. Zatsepin, M. Hikita, C.E. Conrad, G. Nelson, J.D. Coe, S. Basu, T.D. Grant, M.H. Seaberg, R.G. Sierra, et al., Crystal structure of CO-bound cytochrome *c* oxidase determined by serial femtosecond X-ray crystallography at room temperature, Proc. Natl. Acad. Sci. U.S.A. 114 (2017) 8011–8016, https://doi.org/10.1073/pnas.1705628114.

[21] T. Tsukihara, K. Shimokata, Y. Katayama, H. Shimada, K. Muramoto, H. Aoyama, M. Mochizuki, K. Shinzawa-Itoh, E. Yamashita, M. Yao, et al., The low-spin heme of cytochrome *c* oxidase as the driving element of the proton-pumping process, Proc. Natl. Acad. Sci. U.S.A. 100 (2003) 15304–15309, https://doi.org/10.1073/pnas.2635097100.

[22] L. Qin, J. Liu, D.A. Mills, D.A. Proshlyakov, C. Hiser, S. Ferguson-Miller, Redox-dependent conformational changes in cytochrome *c* oxidase suggest a gating mechanism for proton uptake, Biochemistry 48 (2009) 5121–5130, https://doi.org/10.1021/bi9001387.

[23] G. Capitanio, L.L. Palese, F. Papa, S. Papa, Allosteric cooperativity in proton energy conversion in A1-type cytochrome *c* oxidase, J. Mol. Biol. 432 (2020) 534–551, https://doi.org/10.1016/j.jmb.2019.09.027.

[24] S. Han, S. Takahashi, D.L. Rousseau, Time dependence of the catalytic intermediates in cytochrome *c* oxidase, J. Biol. Chem. 275 (2000) 1910–1919, https://doi.org/10.1074/jbc.275.3.1910.

[25] F. Poiana, C. Von Ballmoos, N. Gonska, M.R.A. Blomberg, P. Ädelroth, P. Brzezinski, Splitting of the O-O bond at the heme-copper catalytic site of respiratory oxidase, Sci. Adv. 3 (2017), e1700279. https://doi:10.1126/sciadv.1700279.

[26] A. Maréchal, J.-Y. Xu, N. Genko, A.M. Hartley, F. Haraux, B. Meunier, P.R. Rich, A common coupling mechanism for A-type heme-copper oxidases from bacteria to mitochondria, Proc. Natl. Acad. Sci. U.S.A. 117 (2020) 9349–9355, https://doi.org/10.1073/pnas.2001572117.

[27] S. Arnold, B. Kadenbach, Cell respiration is controlled by ATP, an allosteric inhibitor of cytochrome-*c* oxidase, Eur. J. Biochem. 249 (1997) 350–354, https://doi.org/10.1111/j.1432-1033.1997.t01-1-00350.x.

[28] N. Capitanio, R. Peccarisi, G. Capitanio, G. Villani, E. De Nitto, S. Scacco, S. Papa, Role of nuclear-encoded subunits of mitochondrial cytochrome *c* oxidase in proton pumping revealed by limited enzymatic proteolysis, Biochemistry 33 (1994) 12521–12526, https://doi.org/10.1021/bi00207a020.

[29] R. Acin-Perez, D.L. Gatti, Y. Bai, G. Manfredi, Protein phosphorylation and prevention of cytochrome oxidase inhibition by ATP: coupled mechanisms of energy metabolism regulation, Cell Metabol. 13 (2011) 712–719, https://doi.org/10.1016/j.cmet.2011.03.024.

[30] A.M. Sardanelli, A. Signorile, R. Nuzzi, D. De Rasmo, Z. Technikova-Dobrova, Z. Drahota, A. Occhiello, A. Pica, S. Papa, Occurrence of A-kinase anchor protein and associated cAMP-dependent protein kinase in the inner compartment of mammalian mitochondria, FEBS Lett. 580 (2006) 5690–5696, https://doi.org/10.1016/j.febslet.2006.09.020.

[31] R. Acin-Perez, E. Salazar, M. Kamenetsky, J. Buck, L.R. Levin, G. Manfredi, Cyclic AMP produced inside mitochondria regulates oxidative phosphorylation, Cell Metabol. 9 (2009) 265–276, https://doi.org/10.1016/j.cmet.2009.01.012.

[32] E.A. Berry, M. Guergova-Kuras, L. Huang, A.R. Crofts, Structure and function of cytochrome bc complexes, Annu. Rev. Biochem. 69 (2000) 1005–1075, https://doi.org/10.1146/annurev.biochem.69.1.1005.

[33] A.R. Crofts, J.T. Holland, D. Victoria, D.R.J. Kolling, S.A. Dikanov, R. Gilbreth,

S. Lhee, R. Kuras, M. Guergova Kuras, The Q-cycle reviewed: how well does a monomeric mechanism of the bc_1 complex account for the function of a dimeric complex? Biochim. Biophys. Acta 1777 (2008) 1001–1019, https://doi.org/10.1016/j.bbabio.2008.04.037.
[34] A.R. Crofts, S.W. Rose, R.L. Burton, A.V. Desai, P.J.A. Kenis, S.A. Dikanov, The Q-cycle mechanism of the bc1 complex: a biologist's perspective on atomistic studies, J. Phys. Chem. B 121 (2017) 3701–3717, https://doi.org/10.1021/acs.jpcb.6b10524.
[35] P. Mitchell, Possible molecular mechanisms of the protonmotive function of cytochrome systems, J. Theor. Biol. 62 (1976) 327–367, https://doi.org/10.1016/0022-5193(76)90124-7.
[36] J.A. Letts, K. Fiedorczuk, G. Degliesposti, M. Skehel, L.A. Sazanov, Structures of respiratory supercomplex $I+III_2$ reveal functional and conformational crosstalk, Mol. Cell 75 (2019) 1131–1146, https://doi.org/10.1016/j.molcel.2019.07.022, e6.
[37] M. Lorusso, T. Cocco, D. Boffoli, D. Gatti, S. Meinhardt, T. Ohnishi, S. Papa, Effect of papain digestion on polypeptide subunits and electron transfer pathways in mitochondrial b-c_1 complex, Eur. J. Biochem. 179 (1989) 535–540, https://doi.org/10.1111/j.1432-1033.1989.tb14580.x.
[38] T. Cocco, M. Lorusso, A.M. Sardanelli, M. Minuto, S. Ronchi, G. Tedeschi, S. Papa, Structural and functional characteristics of polypeptide subunits of the bovine heart ubiquinol-cytochrome-c reductase complex, Eur. J. Biochem. 195 (1991) 731–734, https://doi.org/10.1111/j.1432-1033.1991.tb15760.x.
[39] D. Gonzalez-Halphen, M.A. Lindorfer, R.A. Capaldi, Subunit arrangement in beef heart complex III, Biochemistry 27 (1988) 7021–7031, https://doi.org/10.1021/bi00418a053.
[40] T. Ohnishi, B.L. Trumpower, Differential effects of antimycin on ubisemiquinone bound in different environments in isolated succinate-cytochrome c reductase complex, J. Biol. Chem. 255 (1980) 3278–3284, https://doi.org/10.1016/S0021-9258(19)85696-X.
[41] D. Xia, C.A. Yu, H. Kim, J.Z. Xia, A.M. Kachurin, L. Zhang, L. Yu, J. Deisenhofer, Crystal structure of the cytochrome bc1 complex from bovine heart mitochondria, Science 277 (1997) 60–66. https://doi:10.1126/science.277.5322.60.
[42] S. Iwata, J.W. Lee, K. Okada, J.K. Lee, M. Iwata, B. Rasmussen, T.A. Link, S. Ramaswamy, B.K. Jap, Complete structure of the 11-subunit bovine mitochondrial cytochrome bc1 complex, Science 281 (1998) 64–71. https://doi:10.1126/science.281.5373.64.
[43] Z. Zhang, L. Huang, V.M. Shulmeister, Y.I. Chi, K.K. Kim, L.W. Hung, A.R. Crofts, E.A. Berry, S.H. Kim, Electron transfer by domain movement in cytochrome bc_1, Nature 392 (1998) 677–684, https://doi.org/10.1038/33612.
[44] D. Xia, L. Esser, W.K. Tang, F. Zhou, Y. Zhou, L. Yu, C.A. Yu, Structural analysis of cytochrome bc1 complexes: implications to the mechanism of function, Biochim. Biophys. Acta 1827 (2013) 1278–1294, https://doi.org/10.1016/j.bbabio.2012.11.008.
[45] M. Valkova-Valchanova, E. Darrouzet, C.R. Moomaw, C.A. Slaughter, F. Daldal, Proteolytic cleavage of the Fe-S subunit hinge region of *Rhodobacter capsulatus* bc_1 complex: effects of inhibitors and mutations, Biochemistry 39 (2000) 15484–15492, https://doi.org/10.1021/bi000751d.
[46] R. Covian, T. Kleinschroth, B. Ludwig, B.L. Trumpower, Asymmetric binding of stigmatellin to the dimeric *Paracoccus denitrificans* bc_1 complex: *evidence for anti-cooperative ubiquinol oxidation and communication between center P ubiquinol oxidation sites*, J. Biol. Chem. 282 (2007) 22289–22297, https://doi.org/10.1074/jbc.M702132200.
[47] J.W. Cooley, Protein conformational changes involved in the cytochrome bc_1 complex catalytic cycle, Biochim. Biophys. Acta 1827 (2013) 1340–1345, https://doi.org/10.1016/j.bbabio.2013.07.007.
[48] A.M. Barragan, A.R. Crofts, K. Schulten, I.A. Solov'yov, Identification of ubiquinol binding motifs at the Q_o-site of the cytochrome bc_1 complex, J. Phys. Chem. B 119 (2015) 433–447, https://doi.org/10.1021/jp510022w.
[49] M. Sarewicz, M. Dutka, S. Pintscher, A. Osyczka, Triplet state of the semiquinone-Rieske cluster as an intermediate of electronic bifurcation catalyzed by cytochrome bc_1, Biochemistry 52 (2013) 6388–6395, https://doi.org/10.1021/bi400624m.
[50] E.A. Berry, L.S. Huang, Conformationally linked interaction in the cytochrome bc_1 complex between inhibitors of the Q_o site and the Rieske iron-sulfur protein, Biochim. Biophys. Acta 1807 (2011) 1349–1363, https://doi.org/10.1016/j.bbabio.2011.04.005.
[51] C. Lange, C. Hunte, Crystal structure of the yeast cytochrome bc_1 complex with its bound substrate cytochrome c, Proc. Natl. Acad. Sci. U.S.A. 99 (2002) 2800–2805, https://doi.org/10.1073/pnas.052704699.
[52] X. Gao, X. Wen, L. Esser, B. Quinn, L. Yu, C.A. Yu, D. Xia, Structural basis for the quinone reduction in the bc_1 complex: a cooperative analysis of crystal structures of miotchondrial cytochrome bc_1 with bound substrate and inhibitors at the Q_i site, Biochemistry 42 (2003) 9067–9080, https://doi.org/10.1021/bi0341814.
[53] P.A. Postila, K. Kaszuba, P. Kuleta, I. Vattulainen, M. Sarewicz, A. Osyczka, T. Rög, Atomistic determinants of co-enzyme Q reduction at the Q_i-site of the cytochrome bc_1 complex, Sci. Rep. 6 (2016) 33607. https://doi:10.1038/srep33607.
[54] R. Baradaran, J.M. Berrisford, G.S. Minhas, L.A. Sazanov, Crystal structure of the entire respiratory complex I, Nature 494 (2013) 443–448, https://doi.org/10.1038/nature11871.
[55] J. Zhu, K.R. Vinothkumar, J. Hirst, Structure of mammalian respiratory complex I, Nature 536 (2016) 354–358, https://doi.org/10.1038/nature19095.
[56] K. Fiedorczuk, J.A. Letts, G. Degliesposti, K. Kaszuba, M. Skehel, L.A. Sazanov, Atomic structure of the entire mammalian mitochondrial complex I, Nature 538 (2016) 406–410, https://doi.org/10.1038/nature19794.
[57] D. Kampjut, L.A. Sazanov, The coupling mechanism of mammalian respiratory complex I, Science 370 (2020), eabc4209, https://doi.org/10.1126/science.abc4209.
[58] A.S. Galkin, V.G. Grivennikova, A.D. Vinogradov, $\rightarrow H^+/2e^-$ stoichiometry in NADH-quinone reductase reactions catalyzed by bovine heart submitochondrial particles, FEBS Lett. 451 (1999) 157–161, https://doi.org/10.1016/S0014-5793(99)00575-X.
[59] T. Ohnishi, Iron-sulfur clusters/semiquinones in complex I, Biochim. Biophys. Acta 1364 (1998) 186–206, https://doi.org/10.1016/S0005-2728(98)00027-9.
[60] A.D. Vinogradov, V.D. Sled, D.S. Burbaev, V.G. Grivennikova, I.A. Moroz, T. Ohnishi, Energy-dependent complex I-associated ubisemiquinones in submitochondrial particles, FEBS Lett. 370 (1995) 83–87, https://doi.org/10.1016/0014-5793(95)00803-H.
[61] T. Ohnishi, S.T. Ohnishi, K. Shinzawa-Itoh, S. Yoshikawa, Functional role of coenzyme Q in the energy coupling of NADH-CoQ oxidoreductase (complex I): stabilization of the semiquinone state with application of inside-positive membrane potential to proteoliposomes, Biofactors 32 (2008) 13–22, https://doi.org/10.1002/biof.5520320103.
[62] J. Hirst, M.M. Roessler, Energy conversion, redox catalysis and generation of reactive oxygen species by respiratory complex I, Biochim. Biophys. Acta 1857 (2016) 872–883, https://doi.org/10.1016/j.bbabio.2015.12.009.
[63] O. Haapanen, A. Djurabekova, V. Sharma, Role of second quinone binding site in proton pumping by respiratory complex I, Front. Chem. 7 (2019) 221, https://doi.org/10.3389/fchem.2019.00221.
[64] V. Zickermann, C. Wirth, H. Nasiri, K. Siegmund, H. Schwalbe, C. Hunte, U. Brandt, Mechanistic insight from the crystal structure of mitochondrial complex I, Science 347 (2015) 44–49. https://doi:10.1126/science.1259859.
[65] C. Mathiesen, C. Hägerhäll, Transmembrane topology of the NuoL, M and N subunits of NADH:quinone oxidoreductase and their homologues among membrane-bound hydrogenases and bona fide antiporters, Biochim. Biophys. Acta 1556 (2002) 121–132, https://doi.org/10.1016/S0005-2728(02)00343-2.
[66] D.N. Grba, J. Hirst, Mitochondrial complex I structure reveals ordered water molecules for catalysis and proton translocation, Nat. Struct. Mol. Biol. 27 (2020) 892–900, https://doi.org/10.1038/s41594-020-0473-x.
[67] M.E. Mühlbauer, P. Saura, F. Nuber, A. Di Luca, T. Friedrich, V.R.I. Kaila, Water-gated proton transfer dynamics in respiratory complex I, J. Am. Chem. Soc. 142 (2020) 13718–13728, https://doi.org/10.1021/jacs.0c02789.
[68] N. Le Breton, J.J. Wright, A.J.Y. Jones, E. Salvadori, H.R. Bridges, J. Hirst, M.M. Roessler, Using hyperfine electron paramagnetic resonance spectroscopy to define the proton-coupled electron transfer reaction at Fe-S cluster N2 in respiratory complex I, J. Am. Chem. Soc. 139 (2017) 16319–16326, https://doi.org/10.1021/jacs.7b09261.
[69] M. Narayanan, D.J. Gabrieli, S.A. Leung, M.M. Elguindy, C.A. Glaser, N. Saju, S.C. Sinha, E. Nakamaru-Ogiso, Semiquinone and cluster N6 signals in His-tagged proton-translocating NADH:ubiquinone oxidoreductase (complex I) from *Escherichia coli*, J. Biol. Chem. 288 (2013) 14310–14319, https://doi.org/10.1074/jbc.M113.467803.
[70] R. Acin-Perez, P. Fernandez-Silva, M.L. Peleato, A. Perez-Martos, J.A. Enriquez, Respiratory active mitochondrial supercomplexes, Mol. Cell 32 (2008) 529–539, https://doi.org/10.1016/j.molcel.2008.10.021.
[71] M. Wu, J. Gu, R. Guo, Y. Huang, M. Yang, Structure of mammalian respiratory supercomplex $I_1III_2IV_1$, Cell 167 (2016) 1598–1609, https://doi.org/10.1016/j.cell.2016.11.012, e10.
[72] J.A. Letts, L.A. Sazanov, Clarifying the supercomplex: the higher-order organization of the mitochondrial electron transport chain, Nat. Struct. Mol. Biol. 24 (2017) 800–808, https://doi.org/10.1038/nsmb.3460.
[73] I. Wittig, H. Schägger, Supramolecular organization of ATP synthase and respiratory chain in mitochondrial membranes, Biochim. Biophys. Acta 1787 (2009) 672–680, https://doi.org/10.1016/j.bbabio.2008.12.016.
[74] J. Habersetzer, W. Ziani, I. Larrieu, C. Stines-Chaumeil, M.F. Giraud, D. Brèthes, A. Dautant, P. Paumard, ATP synthase oligomerization: from the enzyme models to the mitochondrial morphology, Int. J. Biochem. Cell Biol. 45 (2013) 99–105, https://doi.org/10.1016/j.biocel.2012.05.017.
[75] P. Paumard, J. Vaillier, B. Coulary, J. Schaeffer, V. Soubannier, D.M. Mueller, D. Brèthes, J.P. Di Rago, J. Velours, The ATP synthase is involved in generating mitochondrial cristae morphology, EMBO J. 21 (2002) 221–230, https://doi.org/10.1093/emboj/21.3.221.
[76] L. Scorrano, M. Ashiya, K. Buttle, S. Weiler, S.A. Oakes, C.A. Mannella, S.J. Korsmeyer, A distinct pathway remodels mitochondrial cristae and mobilizes cytochrome c during apoptosis, Dev. Cell 2 (2002) 55–67, https://doi.org/10.1016/S1534-5807(01)00116-2.
[77] A.K. Kondadi, R. Anand, A.S. Reichert, Cristae membrane dynamics – a paradigm change, Trends Cell Biol. 30 (2020) 923–936, https://doi.org/10.1016/j.tcb.2020.08.008.
[78] D. Stock, A.G.W. Leslie, J.E. Walker, Molecular architecture of the rotary motor in ATP synthase, Science 286 (1999) 1700–1705. https://doi:10.1126/science.286.5445.1700.
[79] T.E. Spikes, M.G. Montgomery, J.E. Walker, Structure of the dimeric ATP synthase from bovine mitochondria, Proc. Natl. Acad. Sci. U.S.A. 117 (2020) 23519–23526, https://doi.org/10.1073/pnas.2013998117.
[80] P.C. Hinkle, P/O ratios of mitochondrial oxidative phosphorylation, Biochim. Biophys. Acta 1706 (2005) 1–11, https://doi.org/10.1016/j.bbabio.2004.09.004.

[81] C. Zhang, D.G. Knyazev, Y.A. Vereshaga, E. Ippoliti, T.H. Nguyen, P. Carloni, P. Pohl, Water at hydrophobic interfaces delays proton surface-to-bulk transfer and provides a pathway for lateral proton diffusion, Proc. Natl. Acad. Sci. U.S.A. 109 (2012) 9744–9749, https://doi.org/10.1073/pnas.1121227109.
[82] B. Rieger, W. Junge, K.B. Busch, Lateral pH gradient between OXPHOS complex IV and FoF1 ATP-synthase in folded mitochondrial membranes, Nat. Commun. 5 (2014) 3103, https://doi.org/10.1038/ncomms4103.
[83] D. Ricquier, Respiration uncoupling and metabolism in the control of energy expenditure, Proc. Nutr. Soc. 64 (2005) 47–52, https://doi.org/10.1079/PNS2004408.
[84] S. Papa, N. Capitanio, G. Capitanio, E. De Nitto, M. Minuto, The cytochrome chain of mitochondria exhibits variable H^+/e^- stoichiometry, FEBS Lett. 288 (1991) 183–186, https://doi.org/10.1016/0014-5793(91)81030-C.
[85] N. Capitanio, G. Capitanio, D.A. Demarinis, E. De Nitto, S. Massari, S. Papa, Factors affecting the H^+/e^- stoichiometry in mitochondrial cytochrome c oxidase: influence of the rate of electron flow and transmembrane ΔpH, Biochemistry 35 (1996) 10800–10806, https://doi.org/10.1021/bi9606509.
[86] J. Rydstrom, Mitochondrial NADPH, transhydrogenase and disease, Biochim. Biophys. Acta 1757 (2006) 721–726, https://doi.org/10.1016/j.bbabio.2006.03.010.
[87] S. Papa, M. Lorusso, M. Di Paola, Cooperativity and flexibility of the protonmotive activity of miotchondrial respiratory chain, Biochim. Biophys. Acta 1757 (2006) 428–436, https://doi.org/10.1016/j.bbabio.2006.03.015.
[88] F. Celsi, P. Pizzo, M. Brini, S. Leo, C. Fotino, P. Pinton, R. Rizzuto, Mitochondria, calcium and cell death: a deadly triad in neurodegeneration, Biochim. Biophys. Acta 1787 (2009) 335–344, https://doi.org/10.1016/j.bbabio.2009.02.021.
[89] J.C. Liu, R.J. Parks, J. Liu, J. Stares, I.I. Rovira, E. Murphy, T. Finkel, The in vivo biology of the mitochondrial calcium uniporter, Adv. Exp. Med. Biol. 982 (2017) 49–63, https://doi.org/10.1007/978-3-319-55330-6_3.
[90] S. Papa, D. De Rasmo, Complex I deficiencies in neurological disorders, Trends Mol. Med. 19 (2013) 61–69, https://doi.org/10.1016/j.molmed.2012.11.005.
[91] D. Jimenez-Blasco, A. Busquets-Garcia, E. Hebert-Chatelain, R. Serrat, C. Vicente-Gutierrez, C. Ioannidou, P. Gŏmez-Sotres, I. Lopez-Fabuel, M. Resch-Beusher, E. Resel, et al., Glucose metabolism links astroglial mitochondria to cannabinoid effects, Nature 583 (2020) 603–608, https://doi.org/10.1038/s41586-020-2470-y.
[92] C. Chen, Y. Ko, M. Delannoy, S.J. Ludtke, W. Chiu, P.L. Pedersen, Mitochondrial ATP synthasome: three-dimensional structure by electron microscopy of the ATP synthase in complex formation with carriers for P_i and ADP/ATP*, J. Biol. Chem. 279 (2004) 31761–31768, https://doi.org/10.1074/jbc.M401353200.